Synthesis, Spectral and Quantum Calculation, *in vitro and in silico* Biological Activity Studies of Metal Complexes of a Schiff Base Derived from the Diethyl Pyridine-2,6-Dicarboxylate with Hydrazine

S. M. Rahatul Alam[a], Mohammad Nasir Uddin[a,*], Monir Uddin[a], Wahhida Shumi[b], Sayeda Samina Ahmed[a], Umma Sumia Tohura[a], Md. Moshiur Rahman[a], Emranul Kabir[a] and S. M Iftakharul Alam[a]
[a]*Department of Chemistry, University of Chittagong, Chittagong- 4331, Bangladesh*
[b]*Department of Microbiology, University of Chittagong, Chittagong- 4331, Bangladesh*

Abstract

A Schiff-base (SB) ligand, pyridine-2,6-dicarbohydrazide (PDH), of pyridine-2,6-dicarboxylic acid (PDA) was synthesized via a condensation reaction of hydrazine hydrate (HH) in the presence of concentrated H_2SO_4. Coordination complexes of this SB-ligand with the seven d-block/transition metal (TM) ions, such as chromium (Cr^{3+}), manganese (Mn^{2+}), iron (Fe^{2+}), cobalt (Co^{2+}), nickel (Ni^{2+}), copper (Cu^{2+}), and zinc (Zn^{2+}) ions, were synthesized in a 1:1 (metal: ligand) ratio. All of the prepared compounds were characterized by physicochemical and spectral (UV-Vis, FT-IR, proton NMR, Mass) analyses, along with conductance and magnetic susceptibility studies. A tetrahedral geometry was suspected for seven TM complexes when the SB-ligand acted as a tridentate dibasic ligand. The geometry of the complexes was further confirmed by quantum-chemical (DFT) studies. In vitro and in-silico studies against Salmonella sp., A. niger, Penicillium sp. demonstrated antimicrobial activity. A satisfactory outcome was observed in antioxidant tests for the prepared compounds across all tested concentrations.

Keywords: *Schiff base (SB) ligand, Transition metal complexes, Tetrahedral geometry, Quantum mechanical (QM) calculation, Molecular docking, Anti-microbial and Anti-oxidant activity.*

1. Introduction

Hydrazine derivatives react with carbonyl compounds, producing the condensation product hydrazones, which hold a structural unit like >C=N-N<. Researchers frequently use the hydrazones and their derivatives for their amazing coordination ability. One or more TMs can form coordination compounds with hydrazones, depending on some important factors such as reaction conditions, nature of metals and hydrazines, and ratio of reactants [1]. Six-membered benzene-type ring hydrazones, containing hetero atoms, and their coordination compounds often possess biological efficacy and can disrupt reactions involved with enzymes in the cell [2*3]. Acid hydrazides, R–CO–NH–NH_2, which can act as SB precursors, and their hydrazones, R–CO–NH–N=CH–R', exhibit significant biological activity. Their effectiveness is strongly influenced by the way they coordinate or form complexes with the TM ions that are widely present in biological systems. PDA derivatives exhibit remarkable coordination chemistry [4]. These can act as partially or fully deprotonated particles capable of diverse coordination systems. PDA derivatives are found to be suitable SB-ligands as they are versatile N, O- chelators in coordination chemistry due to their vast coordination modes [5].

* Corresponding author. Tel.: +8801710915011
E-mail address: nasircu72@gmail.com, mnuchem@cu.ac.bd

Manuscript History:
Received 8 September, 2026, Revised 8 October, 2026, Accepted 15 October, 2026, Published 31 October, 2026
Copyright © 2026 UNIMAS Publisher. This is an open access article under the CC BY-NC-SA 4.0 license.
https://doi.org/10.33736/jaspe.14327.2026

e-ISSN: 2289-7771

Dipicolinic acid is found to be present in natural compounds, showing various biological functions and potential pharmacological activities. PDA can interact with several metal ions found in the human body. In recent years, metal complexes derived from PDA derivatives have demonstrated notable antimicrobial activity [6]. The incorporation of metal ions into certain chemical compounds can enhance their antimicrobial properties. Numerous studies have highlighted the significant role of metals in improving antimicrobial activity [1]. Based on the above considerations, the present study demonstrates the synthesis and characterization of PDH and its TM complexes. The quantum mechanical (QM) calculations for these compounds were carried out using Gaussian 09. The SB-ligand and its TM complexes were analysed and characterized by physicochemical studies, such as solubility, melting point (m. p.) determination, spectral studies like UV–Vis, FT-IR, proton NMR (400 MHz), mass, along with molar conductivity (MC) and magnetic susceptibility (MS) studies. Furthermore, the SB-ligand and its TM complexes were evaluated for their antimicrobial efficacy, along with *in-silico* antimicrobial assessments and antioxidant activities.

2. Methods and materials

2.1. Chemicals and apparatus

All reagents and solvents used in these studies were of analytical reagent (AR) grade. PDA, sodium bicarbonate ($NaHCO_3$), and organic solvents, like dimethyl sulphoxide (C_2H_6OS) (DMSO), dimethylformamide (C_3H_7NO) (DMF), acetone (CH_3COCH_3), chloroform ($CHCl_3$), rectified spirit (RS), and absolute ethanol, were procured from Sigma-Aldrich. Hydrazine hydrate ($N_2H_4.H_2O$), chromium(III) chloride hexahydrate ($CrCl_3.6H_2O$), manganese(II) acetate tetrahydrate ($Mn(CH_3COO)_2.4H_2O$), ferrous(II) sulfate heptahydrate ($FeSO_4.7H_2O$), cobalt(II) chloride hexahydrate ($CoCl_2.6H_2O$), nickel(II) chloride hexahydrate ($NiCl_2.6H_2O$), copper(II) nitrate trihydrate ($Cu(NO_3)_2.3H_2O$), zinc(II) nitrate hexahydrate ($Zn(NO_3)_2.6H_2O$), diethyl ether, methanol (CH_3OH), silica gel, calcium chloride hexahydrate ($CaCl_2.6H_2O$), concentrated sulphuric acid (H_2SO_4), standard gallic acid (GA), Folin–Ciocalteu reagent (FCR), and sodium carbonate (Na_2CO_3) were obtained from Merck, Germany. Ethanol was supplied by Duksan Pure Chemicals. Beef extract, peptone, sodium chloride, dextrose, and agar-agar powder were purchased from Qualikems Fine Chem Pvt. Ltd., India. All chemicals were accurately weighed using a four-digit electronic balance (Model AP-002A, SHIMADZU). The melting points (m. p.) of all synthesized TM compounds were estimated using a melting point apparatus (MP-21A, HANNA). Infrared (IR) spectra were recorded as pellets (KBr) over the range of 4000–400 cm^{-1} using an FT-IR spectrophotometer (Prestige-21, SHIMADZU). UV–Vis (electronic) spectra of the synthesized TM compounds were obtained in DMSO within the wavelength range of 200–800 nm using a spectrophotometer (UV-1800, SHIMADZU). The proton NMR spectra were recorded in DMSO at 25°C on a BRUKER NMR (400 MHz) spectrometer. Mass spectral analyses were carried out using a Triple Quadrupole LC/MS system (Agilent 6460). MC (molar conductivity) measurements of the prepared TM complexes (10^{-3} M) in DMSO were recorded using a conductivity meter (HI-8820N, HANNA). MS (magnetic susceptibility) values were determined with a magnetic susceptibility balance manufactured by Sherwood Scientific, Cambridge, UK. For antimicrobial investigations, an autoclave (ALP Co. Ltd., Japan) and a laminar airflow cabinet (BIOQUELL Medical Ltd., UK) were employed. Antifungal activity studies were conducted with pH measurements using a HI-3220 pH meter (HANNA).

2.2. Syntheses

PDA (8.356 g, 50 mmol) was dissolved with the help of 70 mL of ethanol (anhydrous grade) and 2–3 drops of H_2SO_4 (concentrated) and maintained at reflux temperature until a clear solution was obtained. Upon completion, the reaction mixture was poured into cold water (0°C), causing immediate precipitation (ppt) of the solid. A sodium bicarbonate solution was subsequently added until the evolution of gas ceased, indicating complete neutralization. The mixture was then stored at −10 °C for 3–4 days to facilitate crystallization. The resulting ester, diethyl 2,6-pyridinedicarboxylate, was isolated by filtration and washed repeatedly with distilled water (DW). The purified product

exhibited a melting point of 44–46 °C [7-8]. A mixture of diethyl 2,6-pyridinedicarboxylate (11.16 g, 50 mmol) and HH (98%, 2 mL) along with ethanol was heated at reflux conditions for 5 h. Once the reaction had reached completion, roughly 80% of the ethanol was evaporated, after which approximately 20 mL of distilled water (DW) was introduced into the reaction mixture. Then, the reaction mixture was stored at −10 °C for 8 h to promote crystallization. The solid product was subsequently collected by filtration, washed thoroughly with DW, and dried to obtain the desired compound [8].

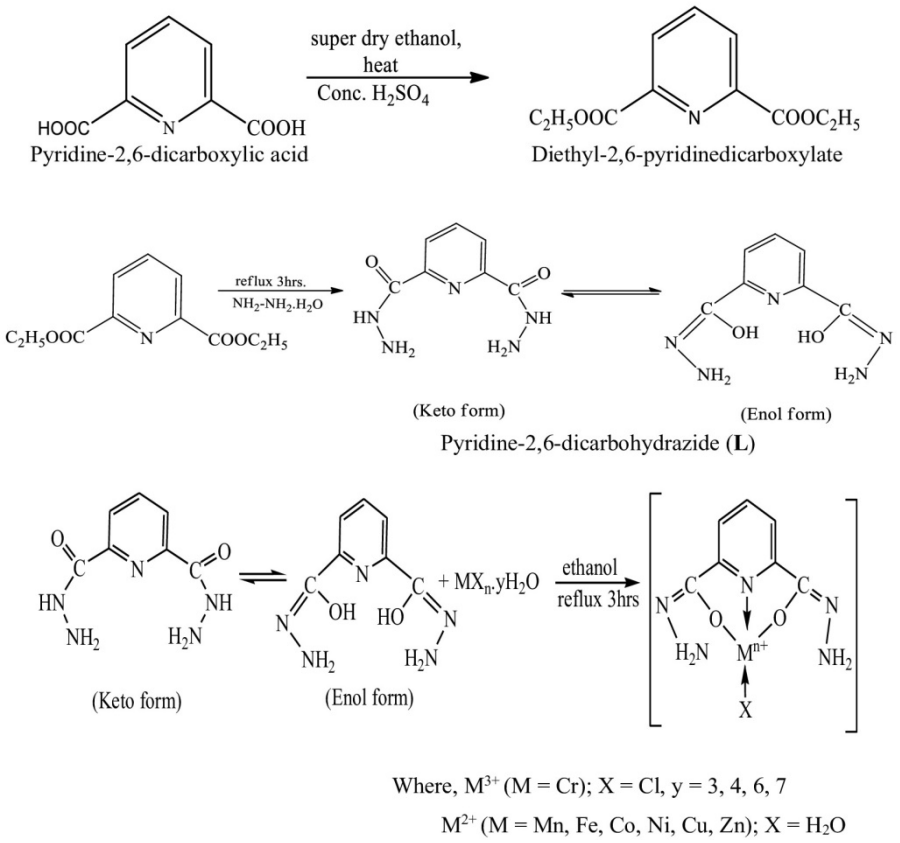


Figure 1. Syntheses of transition metal complexes of pyridine-2,6-dicarbohydrazide

Separate aqueous solutions containing 5 mmol of $CrCl_3.6H_2O$ (1.3322 g), $Mn(CH_3COO)_2.4H_2O$ (1.2255 g), $FeSO_4.7H_2O$ (1.3901 g), $CoCl_2.6H_2O$ (1.1897 g), $NiCl_2.6H_2O$ (1.1885 g), $Cu(NO_3)_2.3H_2O$ (1.2080 g), and $Zn(NO_3)_2.6H_2O$ (1.4875 g) were prepared as metal ion sources. At room temperature (RT), each metal salt solution was introduced dropwise into an ethanolic solution containing the SB ligand (5 mmol, 0.9759 g) dissolved in 30 mL of ethanol, with continuous stirring throughout the addition process. The resulting reaction mixtures were subsequently refluxed for 3 h to facilitate complex formation. Upon completion of the reaction, deep green, light brown, dark brown, ash, green, blue, and white precipitates indicative of the chromium (Cr^{3+}), manganese (Mn^{2+}), iron (Fe^{2+}), cobalt (Co^{2+}), nickel (Ni^{2+}), copper (Cu^{2+}), and zinc (Zn^{2+}) complexes were obtained. After completion of reflux, the resulting dense mixtures were separately dispensed into 100 mL beakers and allowed to cool at RT. The formed solid products (ppt) were separated by filtration, washed with a slight amount of pure ethanol, and then dried to afford the final products. Following drying, the compounds were stored in a desiccator charged with drying agents like silica gel and calcium chloride to maintain dryness before further use. The yields obtained were 69% for Cr, 74% for Mn, 74% for Fe, 72% for Co, 76% for Ni, 71% for Cu, and 77% for Zn. Figure 1 depicts the proposed structures of the synthesized compounds.

2.3. Computational approaches

To obtain reliable values for a variety of energy-related properties, quantum mechanical (QM) computational approaches were employed. These methods are also useful for elucidating the interactions between metal ions and ligands during complex formation. All calculations were performed using the B3LYP functional with the SDD basis set. In this study, computational investigations were conducted within the DFT formalism, using the Becke exchange functional coupled with the *Lee-Yang-Parr* correlational functional [9]. The Gaussian 09 program was used for calculations [4]. Subsequent to geometry optimization, both thermodynamic and electronic characteristics were assessed. The thermodynamic analysis comprised Gibbs free energy, enthalpy, entropy, thermal energy, and dipole moment, whereas the electronic investigation focused on the frontier molecular orbitals- highest occupied molecular orbital (HOMO) and lowest unoccupied molecular orbital (LUMO) and the associated energy gap between them. The PBEPBE/SDD computational approach was further utilized to calculate chemical potential (μ), hardness ($\eta=(E_{LUMO}-E_{HOMO})/2$), and softness ($S=1/\eta$) [10].

2.4. Receptor-protein preparation

The three-dimensional crystal structures of proteins from *Salmonella* species (*6vnt, 6pnv, 1lc5, 6h5g*), *Aspergillus niger* (*1uwc, 3d3z*), and *Penicillium* species (*4f8x, 1bxo, 6pvj, 1m7g, 3a72*) were retrieved from the Protein Data Bank (PDB) and employed as receptor targets for the antimicrobial study [11]. The unwanted molecules were removed using PyMOL software (version 2.2) [4] and were saved as PDB format files for subsequent analysis. The 4.1.0 package of Swiss-Pdb Viewer was used to minimize energy due to optimization of the protein [12]. The keto and enol forms of the optimized SB-ligand (e.g. from the DFT optimization) were utilized in molecular docking investigations.

2.5. Analysis, visualization, and simulation of molecular docking study

Molecular docking simulations and computer-aided drug design approaches were employed to assess the binding affinities and interaction modes between the L and the receptor protein [13]. The PyRx software (version 0.8) was applied to perform the molecular docking studies [14], while non-bonding interactions were analyzed using the 4.5 package of Accelrys Discovery Studio [15]. The YASARA dynamics software refined the molecular docking studies of SB-ligand (L) (both keto and enol forms) through the MD (molecular dynamics) simulations. A periodic boundary condition was applied with a simulation box (e.g., based on the protein dimensions) of 80.56 × 80.56 × 80.56 Å in the x, y, and z directions, respectively. Berendsen thermostat method was utilized to simulate the system for 10 ns, in which pressure-controlled conditions (e.g., 1 bar) were maintained. The MD (molecular dynamics) trajectories were measured at intervals of 10 ps for subsequent analysis.

2.6. Biological applications

All antimicrobial (including antibacterial and antifungal) and antioxidant assays were performed in the Department of Chemistry. The Department of Microbiology of the same university agreed to supply the bacterial and fungal test cultures used in these studies.

2.6.1. Antibacterial activities

A gram-negative bacterium, Salmonella sp. was selected to investigate the antibacterial efficacy of TM compounds. For this purpose, two culture media were utilized: nutrient agar (NA) for the maintenance and preservation of the bacterial strain and nutrient broth (NB) for promoting bacterial growth. The nutrient agar (NA) medium consisted of 3 g beef extract, 3 g peptone, 0.5 g sodium chloride (NaCl), and 15 g agar powder, whereas the nutrient broth (NB) medium had the same composition without agar. Nutrient agar slants were prepared and sterilized by autoclaving. Fresh 24-hour-old bacterial cultures were then inoculated into the prepared sterile slants using sterilized inoculating needles under aseptic conditions. Following inoculation, the cultures were kept under

incubation at approximately 35 ± 2 °C for 24 hours [16]. Ten milliliters of nutrient broth (NB) medium were dispensed into screw-capped test tubes and sterilized using an autoclave. Separate tubes were prepared for each bacterial isolate. After sterilization and cooling, a loopful of 24-hour-old bacterial culture was aseptically transferred into the sterile liquid medium and thoroughly mixed using a vortex mixer to obtain a uniform suspension. This suspension served as the stock culture, with separate preparations maintained for each isolate. Following the liquid culture method, 10 mL of sterile nutrient broth (NB) medium was again prepared in each test tube and autoclaved for 15-20 minutes at 120 °C. Subsequently, 100 microliters of 0.1% test compound (solvent used, DMSO) was dispensed to each tube, followed by inoculation with 100 microliters of the suspension (bacteria) (10 microgram per milliliter). The mixtures were then homogenized and incubated at 37 ± 2 °C for time intervals of 3, 6, 9, 12, 15, 18, 21, and 24 h. A UV–Vis spectrophotometer was utilized to measure absorbance three times, compare with blank (sterile broth) at 650 nm to investigate the bacterial proliferation after each incubation period.

2.6.2. Antifungal activities

Two fungi were chosen, named as A. niger and *Penicillium sp.,* to investigate antifungal efficacy against the synthesized L and its TM complexes. A significant efficacy was observed against the selected fungi. This investigation was conducted using the liquid culture method (LCM). Antifungal efficacy was assessed by measuring changes in pH and fungal biomass weight. Since fungal growth is accompanied by the production of organic acids (e.g., citric, gluconic), a drop in pH serves as an indicator of metabolic activity. Inhibition of growth by the test compounds is therefore reflected in a smaller pH decrease compared with the control. Throughout the study, the PDA (potato dextrose agar) medium was used for the cultivation and maintenance of the isolated fungal strains. For antifungal efficacy, potato dextrose liquid (PDL) medium, which has the same composition as PDA but lacks agar, was employed [17]. The PDA medium was prepared using DW (1000 mL), 200 g of potatoes, 20 g of dextrose, and 15 g of agar. Sliced potatoes (200 g) were boiled in DW, and the resulting extract was collected by decantation. The extract was dispensed into a beaker (1000 mL) and diluted to the required volume with DW. Dextrose (20 g) was then gradually added and thoroughly mixed with the help of a glass rod. A 250 mL conical flask was used to add the experimental medium and boil it for 10 min, then autoclaved to sterilize at 121 °C under 15 psi. The sterilized PDA medium was subsequently used for the cultivation and maintenance of the fungal isolates. A small amount of mycelial growth from the fungal cultures was aseptically transferred onto freshly prepared PDA slants using sterilized inoculating needles. At 27 ± 2 °C, the inoculated slants were incubated to sterilize for 3–7 days. For antifungal efficacy testing, 50 mL of PDL medium was dispensed into separate conical flasks (150 mL) after sterilization. Subsequently, 100 µL of each test compound (0.1% concentration) and 100 microliters of fungal suspension were added to the respective flasks and mixed thoroughly. The flasks were sealed with cotton plugs and kept under incubation to sterilize at approximately 27 ± 2 °C for three days for *A. niger* and seven days for *Penicillium sp*. The fungal biomass was separated by filtration, and the pH of the filtrate was measured after the end of the incubation. The collected biomass was kept at 60–70 °C to dry overnight and subsequently weighed to determine fungal growth.

2.6.3. Antioxidant activities

The antioxidant efficacies were determined by absorbance calculation at a wavelength 760 nm using FCR at different concentrations with the help of phenolic content (PC) determination [4]. Standard gallic acid (GA) was used to draw a calibration (cal.) curve to estimate the net amount of phenol, in which TPC was represented as GA equivalents (GAE). The net phenolic amount was calculated from the corresponding linear regression equation and reported as micrograms (µg) of GA equivalent per gram of dry analyte mass (µg GAE/g). For the assay, 1 milliliter of every tested sample solution was dispensed into a test tube containing 5 milliliters of FCR and diluted 10 times with DW. Following this, 2.5 mL of 7.5% sodium carbonate (Na_2CO_3) solution was added, and the mixture was carefully mixed for further study. The test tube was incubated for sterilization for 20 minutes at 250 °C to complete the reaction. Then, the absorbance of the solution was measured at 760 nm using a UV spectrophotometer against a blank. The net phenolic amount in tested samples as GA equivalents

(GAE) was calculated as follows: C = (c×V)/m (where, C= net phenolic amount, mg g^{-1} of tested sample, as GAE; c = the concentration of GA established from the cal. curve, µg mL^{-1}; V = the volume of tested sample solution, mL; m = weight of tested sample in gram, g).

3. Results and discussion

3.1. Physical properties

In this study, the synthesized L and its TM complexes were colored with high melting points (> 300 °C). The m. p. of the L was less than that of the prepared TM complexes. Both the L and TM complexes were quite stable at RT and can be stored for a long time. These were insoluble in DW but completely soluble in DMSO. That is why DMSO was used as the solvent for characterizations. It is clear from the color formation (Table 1) that the complexes were formed.

Table 1. The elemental analysis and physical data of compounds studied.

Compd	MF	Elemental Analysis (%)				M. P. (°C)	Color	% Yield
		M	C	H	N			
L	LH_2	--	42.89 (43.02)	5.52 (5.62)	35.78 (35.91)	>320	White	80
C1	[Cr(L)Cl]	18.52 (18.39)	29.88 (29.71)	4.03 (3.91)	24.67 (24.81)	>340	Dark green	69
C2	[Mn(L)(H_2O)]	20.67 (20.48)	31.46 (31.31)	4.31 (4.13)	25.99 (26.15)	>340	Light Brown	74
C3	[Fe(L)(H_2O)]	20.82 (20.76)	30.95 (31.21)	3.93 (4.07)	26.12 (26.02)	>340	Dark Brown	74
C4	[Co(L)(H_2O)]	21.78 (21.65)	31.14 (30.90)	4.15 (4.03)	26.02 (25.78)	265	Ash	72
C5	[Ni(L)(H_2O)]	20.95 (21.58)	30.85 (30.92)	4.25 (4.10)	25.98 (25.72)	274	Green	76
C6	[Cu(L)(H_2O)]	23.36 (23.92)	30.56 (30.73)	3.92 (4.02)	25.45 (25.56)	306	Blue	71
C7	[Zn(L)(H_2O)]	22.99 (23.61)	30.31 (30.15)	4.14 (4.01)	23.11 (25.32)	>340	White	77

*Molecular formula = MF; M. P. = Melting point

3.2. Spectral characterization of the studied compounds

3.2.1. Infra-red spectra

Infrared (IR) spectroscopy provides crucial insights into the nature of the functional groups involved in synthesized TM complexes. Table 2 represents the major infrared absorption bands. Analysis of the IR spectra (Supplementary Figure 1) revealed a broad absorption band in the range of 3250–3500 cm^{-1}, which is characteristic of the stretching vibrations of coordinated water molecules present in the complexes [18]. A highly intense absorption band at 1633 cm^{-1} for the free SB-ligand is associated with azomethine C=N stretching. The changing of this group to a suppressed frequency in the TM metal complexes when compared to the L supports the coordination of the TM metal ion through the nitrogen (N) atom of the azomethine group [14]. A metal atom would scale down the electron density in the azomethine link and thus suppress the –HC=N absorption. The L shows a declining trend of 15-35 cm^{-1}, due to an absorption peak of carbon-nitrogen double bond (νC=N), implying the involvement of the nitrogen of the azomethine group in coordination. The spectral band identified at approximately 1600 cm^{-1} can be ascribed to the stretching vibration of the conjugated >C=N–N< linkage. [19], pointing to the enolization of the L in the presence of metal ions and the participation of the enolic oxygen in coordination. The absorption bands detected at 1290-1330 cm^{-1}

have been ascribed to phenolic/enolic carbon-oxygen single bond. The TM metal complexes corroborate the ν(C–N) stretching vibration at higher frequencies compared with that of the L, implying the coordination of the L to the TM metal center. Based on previously reported metal isotope substitution studies as well as ^{15}N and ^{18}O isotope labeling investigations, the absorption bands observed in the ranges of 506–600 cm^{-1} and 400–470 cm^{-1} were putatively designated to metal-nitrogen (M-N) and metal-oxygen (M-O) stretching vibrations, respectively. The presence of these significant metal–nitrogen (M-N) and metal–oxygen (M-O) bands substantiates the participation of nitrogen and oxygen donor atoms in the coordination process with the investigated TM metal ions.

Table 2. Significant IR bands (cm^{-1}) for the tested compounds.

Compound	υO-H/ υH_2O	υN-H	υC=N	υC=C[a]	υC-N	υN-N	υM-O	υM-N
L	3350w	3087w	1633vs	1568ms	1396ms	1081ms	-	-
C1	3468w	3142w	1600vs	1578ms	1379ms	1086vs	539ms	437s
C2	3368w	3231w	1616vs	1587vs	1395ms	1015s	530s	429ms
C3	3401w	3242w	1600vs	1539s	1376s	1033s	526s	435s
C4	3391w	3086w	1612vs	1573ms	1395ms	1078s	541w	430w
C5	3367w	3015w	1610vs	1431s	1380ms	1037s	544w	418s
C6	3417w	3061w	1596vs	1644vs	1370ms	1080s	510w	435ms
C7	3401w	3160w	1612vs	1567s	1393ms	1078s	599s	428s

Where, '[a] = aromatic, vs = very strong, ms = medium strong, s = strong, w = weak'

3.2.2. ^{1}H NMR (Nuclear Magnetic Resonance) spectra

^{1}H NMR spectra of the L (Supplementary Figure 2) and C5 (Supplementary Figure 3) were recorded in DMSO-d6 at 25 °C using tetramethylsilane (TMS) as an internal standard at 400 MHz. The ^{1}H NMR spectra of the C5 complex was recorded as a representative complex because C1-C6 complexes are paramagnetic which are proved from the magnetic moment value (Table 3). The L exhibits a peak at 2.5 ppm, for the amino (-NH_2) protonic peak, which is observed generally 4.0-5.0 ppm. It fluctuates due to moisture or solvent. Due to moisture content in the DMSO-d6, a broad water peak appeared at 3.35 ppm, distinct from the standard solvent residual peak at 2.50 ppm. The spectrum also shows a singlet peak at 7.89 and 7.92 ppm for –NH/-OH which is merged and split. In this regard, the -NH- group is predominant in keto form of the SB ligand but -OH group is predominant in enolic form [20], and another peak of Ar-H (multiplet, 3H, pyridine) is observed at 6.92-7.10 ppm. The absence of the singlet resonance corresponding to the hydroxy (–OH) proton in the proton NMR spectrum of the complex suggests that the oxygen (O) atoms in the enolic form of the ligand coordinate to the metal center (C5) through deprotonation. The aromatic proton (Ar–H) signals appeared as multiplets in the region of 6.92–7.10 ppm and shifted slightly downfield by 0.05 ppm upon complexation, indicating that these protons were not significantly affected by the chelation process [21].

3.2.3. Mass Spectra

The mass spectrum of SB-ligand (L) (Supplementary Figure 4) and its two of the complexes, one is C6 (Figure 2) and another is C7 (Supplementary Figure 5) show molecular ion peak at m/z = 194.93, m/z = 274.01 and m/z = 276.77 (Table 3) respectively, which correspond to the molecular mass of the respective compound. This supports the structure of the ligand and complexes and confirms the ML type stoichiometry of the metal chelates; tetrahedral geometrical shapes were presumed for the complexes. The series of peaks in the ranges of 78.93, 118.93, 160.93, and 194.93 may correspond to various fragments of the SB-ligand, and their intensity gives an idea of the stability of the fragments. Another series of peaks in the ranges of 78.93, 118.93, 160.93, 194.93, and 274.01 may correspond to various fragments of the copper (Cu-II) complex, and their intensity gives an idea of the stability of the fragments. The peaks at 78.93, 118.93, 160.93, 194.93, and 276.77 may be

related to various fragments of the zinc (Zn-II) complex, and their intensities indicate the stability of these fragments. Some unavoidable errors, like spectrum recording, the presence of impurities, and isotopic abundance of the atoms in the sample, a higher ionization potential can cause a small distortion of m/z, $[M \pm 1]^+$, $[M \pm 2]^+$ of the molecular ion peaks [22-23].

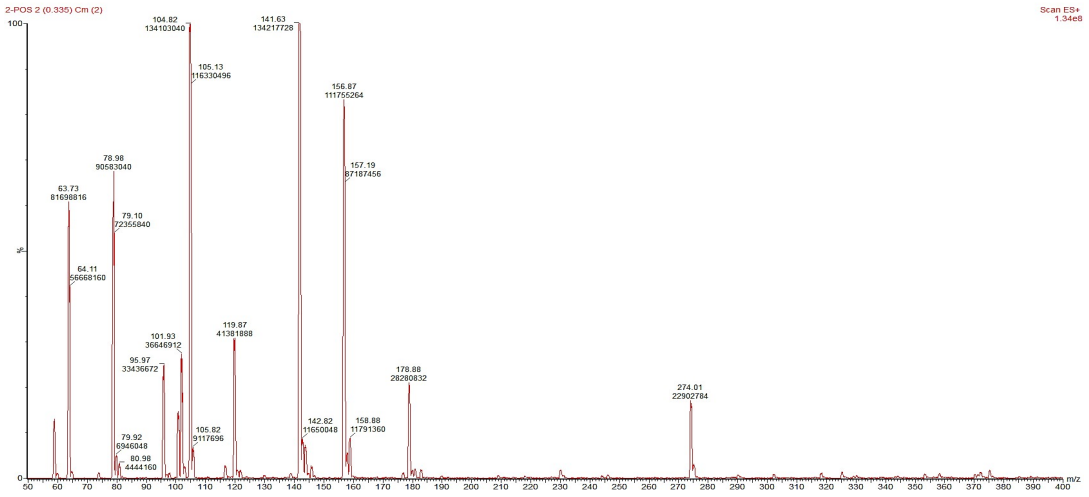


Figure 2. Mass spectrum of complex, C6

3.2.4. Electronic (UV-Vis) Spectra

The electronic (UV-Vis) spectra (800 nm to 200 nm) of all the compounds (10^{-3} M solution) were obtained in DMSO (Supplementary Figure 6). Table 3 represents the spectral information. The complexes show bands (Table 3) near the visible region, which may be ligand or charge-transfer spectra. These electronic spectra show bands in the region 200-420 nm due to charge transfer only. This shift may be characteristic of the donation of the lone pairs of the nitrogen atoms of the SB-ligand to the metal ion (N-M). A similar observation was obtained for the prepared complexes. C1 displays bands at 340 nm (29412 cm^{-1}) corresponding to $^4A_2(F) \rightarrow {}^4T_1(P)$ (ν_3), indicating the tetrahedral geometry. The SB-ligand (L) peaks were around 256, 269 nm (aryl π-π* and imino π-π* (-C=N-) transitions, respectively) [24]. C4 shows an absorption band at 353 nm, which is correlated with the complex in a tetrahedral geometry. All the above compounds show bands at 269 nm [imino π-π* (-C=N) transitions] and bands at 306-357 nm (charge transfer/ intra-ligand transitions). From this, it must be predicted that the complexes formed with the synthesized SB-ligand may be tetrahedral in geometry.

3.2.5. Conductivity and magnetic properties

The MC measurements of the TM complexes were carried out in DMSO solution. All complexes exhibited relatively low MC values, indicating their non-electrolytic nature [25]. These results suggest the absence of free inorganic anions outside the coordination sphere, confirming that the anions, if present, are coordinated within the metal complexes. The conductance measurements indicate that the synthesized PDH-derived TM complexes are non-electrolytic in nature. The low molar conductance values suggest the absence of free anions outside the coordination sphere, thereby supporting the predicted structures of all the complexes (Table 3). The magnetic susceptibility data of the synthesized complexes are also presented in Table 3. Among them, the C7 complex exhibited diamagnetic behavior, as evidenced by its zero magnetic moment value, indicating the absence of unpaired electrons. Furthermore, analysis of the magnetic moment data suggests that the C2 complex

possesses a tetrahedral geometry [26]. The magnetic moment values of complexes C1, C2, C3, C4, C5, and C6 were found to be 3.89, 5.92, 5.30, 4.77, 3.32, and 1.91 B.M., respectively. The C1 complex exhibited a magnetic moment of 3.89 B.M., which corresponds to the presence of three unpaired electrons. Based on the magnetic susceptibility data, the C1 complex is proposed to possess a high-spin tetrahedral configuration. According to literature reports, a magnetic moment in the range of 3.7–3.9 B.M. is characteristic of tetrahedral geometry for the C1 complex. The C4 complex exhibited a magnetic moment of 4.77 B.M., which also falls within the typical range of 4.7–5.2 B.M. expected for tetrahedral coordination. The C6 complex showed a magnetic moment of 1.91 B.M., corresponding to a single unpaired electron with a slight orbital contribution to the spin-only value and minimal spin–spin interactions. For the C2, C3, C4, and C5 complexes, the observed magnetic moment values were 5.92, 5.30, 4.77, 3.32, and 1.91 B.M., respectively. Based on these magnetic data, a tetrahedral geometry can be reasonably predicted for all of the synthesized TM complexes.

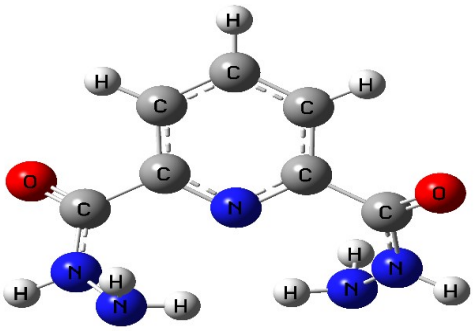
Table 3. UV-Vis and Mass spectral data, magnetic moments and conductance values of complexes.

Compound	Wavelength (nm)	Magnetic moment (B.M)	M. weight	m/z	Conductance ($ohm^{-1}cm^2mol^{-1}$)
					Molar conductance
Cr-d^4 (C1)	340, 269	3.89 (t_{2g}^3 e_g^1)	282.7	281.2	4.85
Mn-d^5 (C2)	353, 345, 269	5.92(t_{2g}^4 e_g^1)	268.2	269.2	3.88
Fe-d^6 (C3)	343, 269	5.30 (t_{2g}^3 e_g^3)	269.0	270.01	6.25
Co-d^7 (C4)	353, 269	4.77 (t_{2g}^4 e_g^3)	272.1	272.8	14.55
Ni-d^8 (C5)	306, 269	3.32 (t_{2g}^4 e_g^4)	271.9	272.2	22.31
Cu-d^9 (C6)	357, 269	1.91 (t_{2g}^4 e_g^5)	274.0	274.0	2.91
Zn-d^{10} (C7)	347, 269	0.00 (t_{2g}^6 e_g^4)	276.8	276.77	6.79

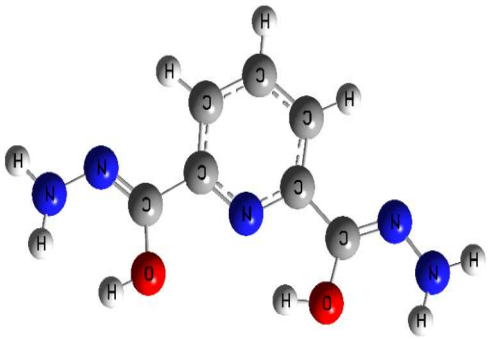
3.3. Quantum mechanical calculation

3.3.1. Optimization condition of ligand and complexes

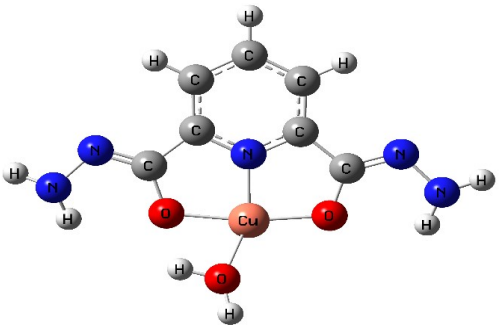
QM calculation is a crucial tool in Chemistry, utilized in the design of L and TM complexes based on preceding characterization data from IR, proton NMR, Mass, and UV–Vis spectra. This calculation aimed to compare the results with theoretical values. The calculation of the different types of energies and the interpretation of various types of complex interactions between L and TM in the formation of complexes are permitted by the QM methods. The QM methods appropriately explain important molecular properties such as stability, reactivity, thermodynamics, electrical, and geometrical properties. The investigated data observed in this study support fantabulous ground-state geometries. During the geometry optimizations, the structures were not restricted. The geometry of L, C1, C6, and C7 was optimized by QM calculations following their geometry, characterized by IR, ^{1}H NMR, Mass, and UV–Vis. The optimized features of L, C1, C6, and C7 are represented in Figure 3.



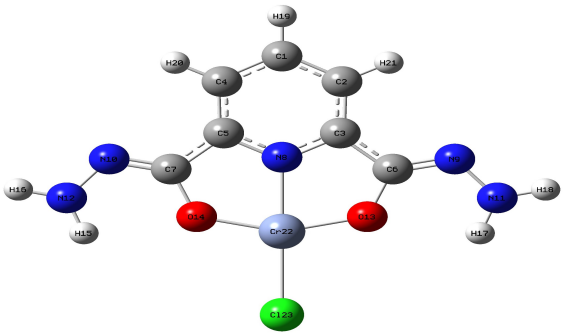
Optimized structure of L-Keto



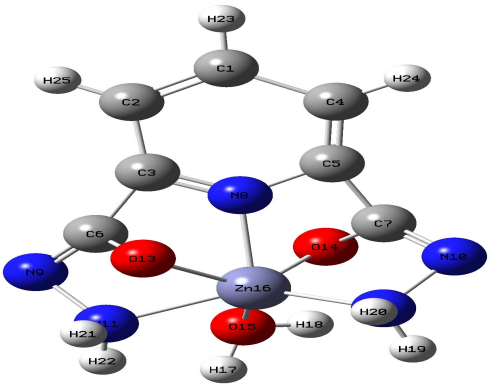
Optimized structure of L-Enol



Optimized structure of C1



Optimized structure of C6



Optimized structure of C7

Figure 3. Optimized structure of Ligand, L (Enol/Keto) and complexes, C1, C6, C7

3.3.2. Thermochemistry

The two important properties, like stability and reactivity of molecules, can be illustrated by the thermochemical study. The free energy, enthalpy, and dipole moment of L ((Enol/Keto), C1, C6, C7) are reported in Table 4. In this study, the negative results indicate that compounds are more stable energetically as well as configurationally. The most negative results of the thermochemical properties for C1, C6, and C7 complexes were comparable to those of the L (Enol/Keto), observed by the DFT computation, which displayed greater thermal stability. Similarly, the enol form of L, C1, and C6 was confirmed to be more polar than the other form of L and C7 from DFT calculations, having a larger dipole moment than the others. C7 is chemically or thermally more stable, while C1 has a higher dipole moment due to its greater polarity.

Table 4. Molecular formula, Molecular weight (g/mol), enthalpy (Hartree), Gibb's free energies (Hartree), and Dipole moment (Debye) of the investigated ligand and complexes.

Name	MF	MW	En.	GFE	DM
L-Enol	$L\underline{H_2}$	195.20	-696.1227	-696.1749	3.4854
L-Keto	$L\underline{H_2}$	195.20	-696.1464	-696.2011	1.4885
C1	$C_7H_7N_5O_2CrCl$	282.70	-2188.6855	-2188.7448	6.5531
C6	$C_7H_9N_5O_3Cu$	274.01	-2399.7802	-2399.8386	3.4239
C7	$C_7H_9N_5O_3Zn$	276.77	-2537.9624	-2538.0189	2.3449

*Molecular formula = MF; Molecular weight = MW; Enthalpy = En.; Gibb's free energy = GFE; Dipole moment = DM.

Table 5. Energy gaps ($\Delta\varepsilon$) between HOMO and LUMO (eV), chemical potential (μ), hardness (η), softness (S) of the studied ligand and complexes.

Name	υHOMO	υLUMO	$\Delta\varepsilon$	μ	η	S
L-Enol	-4.8031	-0.9010	3.9021	-2.8521	1.9511	0.5125
L-Keto	-6.6940	-1.8096	4.8844	-4.2518	2.4422	0.4095
C1	-4.4673	-1.1389	3.3284	-2.8031	1.6642	0.6009
C6	-4.4238	-1.1889	3.2349	-2.8064	1.6175	0.6182
C7	-4.6115	-1.2738	3.3377	-2.9427	1.6689	0.5992

3.3.3. Frontier molecular orbital (FMO)

Orbital analysis is crucial for predicting the energy requirements of chemical reactions. By determining the highest occupied molecular orbital (HOMO) and the lowest unoccupied molecular orbital (LUMO), insights into various reactions can be gained [27, 28]. Orbital analysis is crucial for predicting the energy requirements of chemical reactions. By determining the highest occupied molecular orbital (HOMO) and the lowest unoccupied molecular orbital (LUMO), insights into various reactions can be gained [29,30]. The chemical hardness and softness of any molecule can be illustrated by the HOMO-LUMO energy variation ($\Delta\mathcal{E}$). A larger $\Delta\mathcal{E}$ reflects improved kinetic stability and lower chemical reactivity [31]. Density functional theory (Gaussian 09) calculated the chemical hardness, softness, and the difference between HOMO and LUMO of L (Enol/Keto), C1, C6, and C7 (Table 5). In the DFT method, the keto form of the L showed the highest, and C6 showed the lowest difference between HOMO and LUMO. The higher softness of C6 indicated higher chemical reactivity. The $\Delta\mathcal{E}$ of L, C6 is represented in Figure 4. C6 showed a lower $\Delta\mathcal{E}$ and higher softness, which can result in the manifestation of improved chemical activity than C7 [32]. The lower polarizability and reactivity of L are observed due to its reduced softness. The experimental data for L indicate that it has the possibility to perform as a dibasic tridentate ligand in complex formation. Hence, a tetrahedral geometry for the complexes (C1-C7) was proposed. All complexes displayed stability, which were mostly insoluble in water as well as organic solvents, but soluble or slightly soluble in DMSO/DMF. Table 1 shows that many of the compounds had a melting point greater than 250°C. The optimized ligand and all the complexes exhibited thermal stability, and complexes (C1-C7) were chemically more polar as well as more reactive than the ligand. From all of these evidences, the assumed mononuclear or monometallic structure of the synthesized compounds.

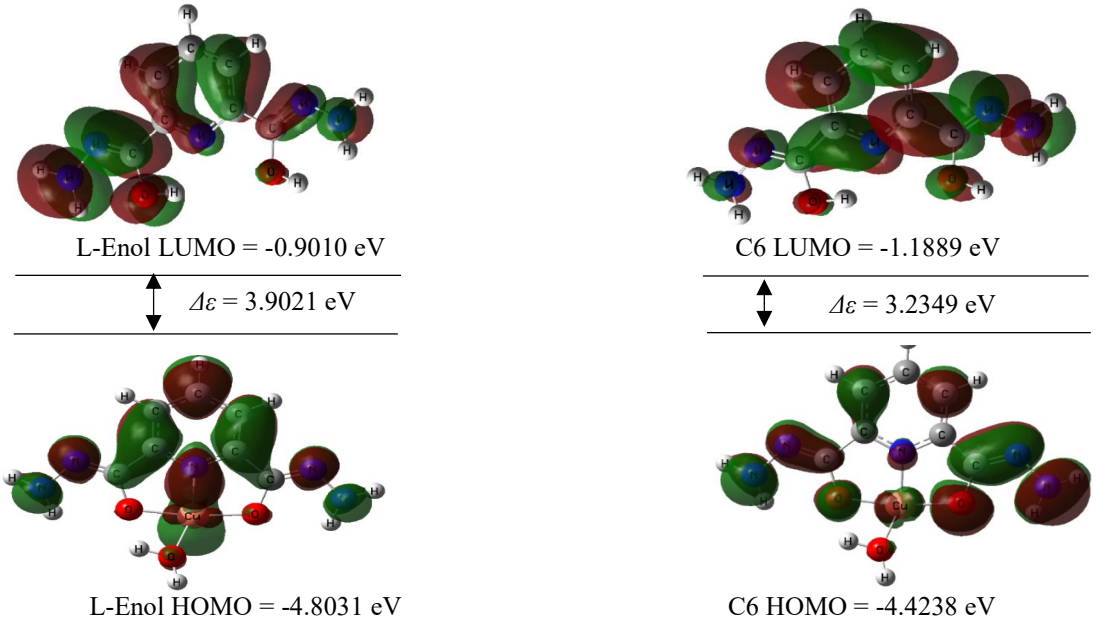


Figure 4. Frontier molecular orbital features of L (Enol/Keto), C6

3.3.4. Molecular electrostatic potential (MEP)

Determining MEP (molecular electrostatic potential) contributes to elucidating the likely sites for biological recognition process, electrophilic and nucleophilic attacks and H-bonding interactions [33]. The electrophilic attack is observed in the electronegative site, which is denoted by red color. In contrast, the nucleophilic attack is observed in the electropositive site, represented by blue color. The MEP value indicates that the C7 complex shows the highest negative result (-0.1373 a.u.) for the oxygen atom and the maximum positive value (+0.1568 a.u.) for the hydrogen atom; the L-Enol shows +0.1824 a.u. for hydrogen and -0.1417 a.u. for the oxygen atom, and L-Keto shows +0.1583 a.u. for hydrogen and -0.2330 a.u. for the oxygen atom (Figure 5).

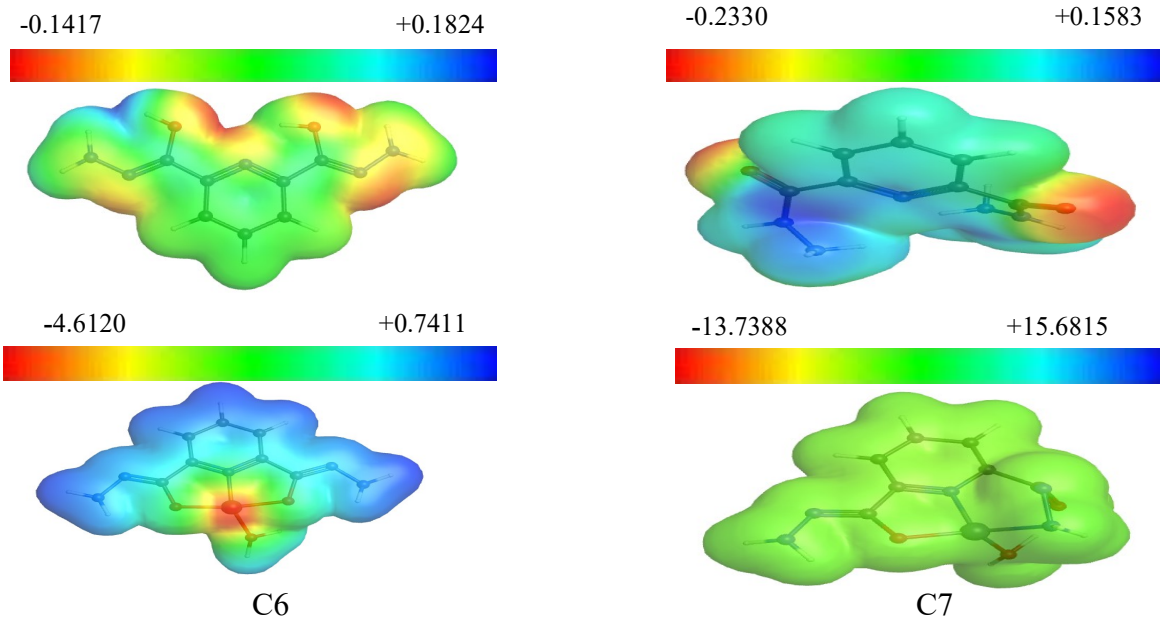


Figure 5. Molecular electrostatic potential of L (Enol/Keto), C6 and C7

3.3.5. Vibrational frequency

The interaction between infrared radiation (400-4000 cm^{-1}) and experimental compounds is discussed in vibrational spectroscopy. The spectrum of the ligand (Fig 6) derived from this spectroscopy helps to signify various functional groups in the tested compounds [34]. IR bands from QM calculation (Table 6) of various significant bands like C-O, C═C, C═O, and C═N were correlated with those of the investigated results of L and C6 (Table 2). The frequencies obtained in wavenumber were scaled by multiplying by the scaling factor (0.9688). The bands observed at 1715, 1635, 1450, 1300, and 1160 cm^{-1} due to C═O, C═N, C═C, and C-O of the aryl/keto ethylenic groups followed the corresponding experimental bands at 1684, 1605, 1452, 1291, and 1218 cm^{-1}, respectively.

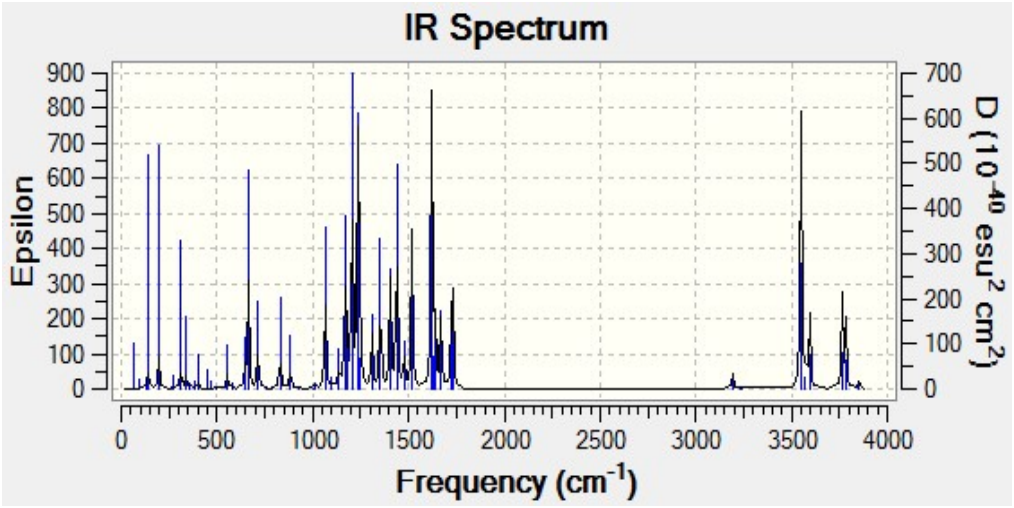


Figure 6. Theoretical IR spectrum of Ligand

Table 6. Theoretical vibrational frequencies of the investigated compounds.

Compound Name	Assignment	Theoretical frequency (cm^{-1})	Experimental frequency (cm^{-1})
L	νO-H	3540	3350
	νC-O	1260	1276
	νC═N	1660	1633
	νC═C	1590	1568
C6	νO-H	3380	3417
	νC-O	1245	1269
	νC═N	1670	1596
	νC═C	1680	1644

3.3.6. Biological applications

3.3.6.1 Antibacterial efficacy

The bacterial proliferation from 0 to 24 hours of culture at 37±2 °C in the presence of the C7 complex is shown in Figure 7. For all the compounds under analysis, the optical density for Salmonella sp. was determined. It is noticed from Figure 7 that the bacterial growth is increased after a certain time period, which is ensured by the calculation of absorbance at 650 nm.

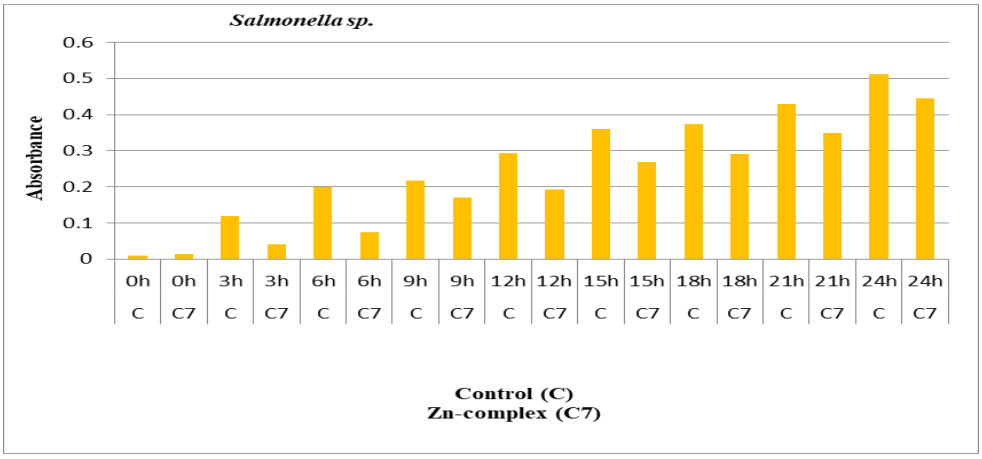
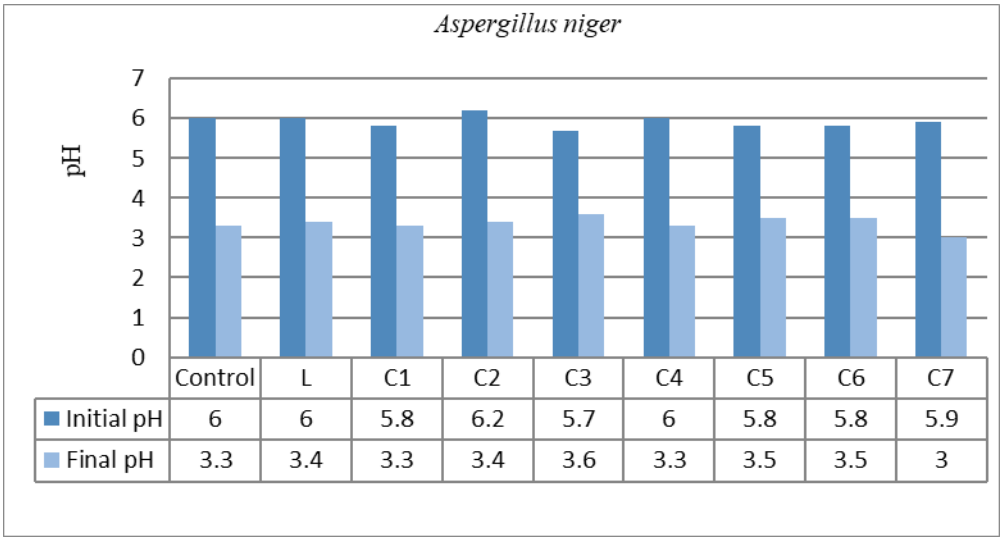


Figure 7. Antibacterial activity of C7 compound against *Salmonella sp.*

The growth of the control is always higher than that of the investigated compounds. After each time period, the measured absorbance of the tested compounds was lower than that of the control. This is because the tested compounds affect the cell membrane of the bacteria, resulting in less turbidity of the solution, which indicates their inhibiting capacity against *Salmonella sp.* Of them, the C1 complex showed the highest antibacterial efficacy than the rest of the compounds. The decreasing order of the antibacterial activities of the compounds is: C1>C2>C7>C4>C5> C6>L>C3.

3.3.6.2 Antifungal efficacy

The photographic images and biomass weight of the tested fungi, A. niger and Penicillium sp., showed a larger amount of fungal growth in the positive control than in the tested compounds. Figure 8 (pH measurement) represents the antifungal activity against A. niger. From this investigation, it is observed that, SB ligand and C2, C3, C5, C6 showed inhibitory activities against A. niger. On the other hand, inhibitory activities of all the synthesized compounds L and C1-C7 were also observed for another fungus, Penicillium sp. Photographic images showed that the tested chemicals containing fungi were present in smaller amounts than the positive control, indicating the activities against the investigated fungus of the L and TM complexes. The pH measurement data showed that more fungal growth indicates lower pH values and less fungal growth indicates higher pH values. In contrast, biomass measurement data verified that the fungi-containing tested compounds weighed less than compared to the positive control (which contained no compounds). According to the above information, it is evident that the synthesized L and TM complexes showed antifungal activities.



	Control	L	C1	C2	C3	C4	C5	C6	C7
Initial pH	6	6	5.8	6.2	5.7	6	5.8	5.8	5.9
Final pH	3.3	3.4	3.3	3.4	3.6	3.3	3.5	3.5	3

Figure 8. Antifungal activity of L, C1-C7 compounds against *Aspergillus niger*

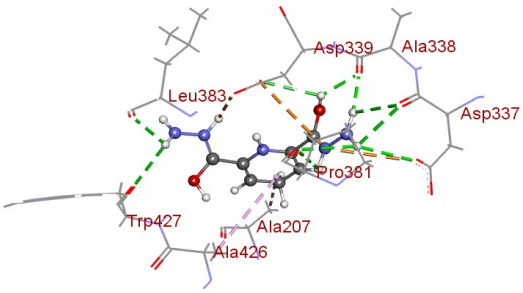
3.3.7. Molecular docking and nonbonding analysis

3.3.7.1. In silico antibacterial activities

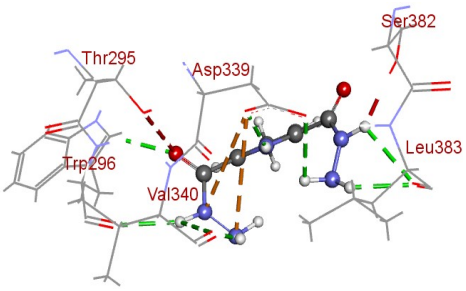
The process of multiple molecules interacting to form stable adducts is known as molecular docking, and it is utilized in standard bioremediation, hit detection, logical drug design and lead optimization [14]. In Supplementary Table 1, the antibacterial activities of the examined compounds against *Salmonella sp*. are given. The negative binding affinity of the investigated compounds, like L-Enol and L-Keto, with receptor proteins of Gram-negative bacteria such as *Salmonella sp*. is represented in table 7, indicating stronger binding between them. In non-bonding interactions, halogen bonds, hydrogen bonds, and hydrophobic bonds are also involved. Supplementary Table 1 shows that the stability order of the compounds with the receptor protein is 6vnt>6pnv>1lc5>6h5g, with binding affinities of -7.5, -7.3, -7.0, and -6.8, respectively. Strong H-bonding, i.e., ≤ 2.3 Å, increases the binding affinity [35, 36]. Supplementary Figure 6 depicts the non-bonding interactions with various receptor proteins.

3.3.7.2. In silico antifungal activities

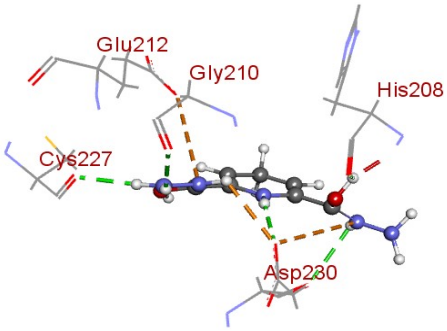
In our investigation, the strongest binding score of L-Keto with the receptor-protein (e.g., 6vnt) is specifically an H-bond with ASP124 at a distance of 1.99 Å. Table 7 represents the antifungal activities against *A. niger and Penicillium sp*. The higher binding affinity of L-Keto with the 4f8x receptor protein of *Penicillium sp.* is due to LYS76, H(2.13). Moreover, except for hydrogen bonds, the compounds are also bonded to various receptor proteins by attractive charge, carbon-hydrogen bond, alkyl, salt bridge, p-alkyl, etc. Almost all of the residues of the receptor proteins of *Salmonella sp., A. niger, and Penicillium sp.* are represented in Table 7. The figures of the nonbonding interaction with (a) *Salmonella sp.* (6pnv), (b) *A. niger* (1uwc), and (c) *Penicillium sp.* (4f8x) are shown in Fig 9. To investigate structural properties, flexibility, and binding mechanism of the L with 6pnv, a molecular dynamics (MD) (10 ns) simulation for the protein-L complex, and the protein without ligand, was performed. The root-mean-square deviation (RMSD) was calculated throughout the simulations. RMSD analysis clearly showed that 6pnv-L complex was more flexible than its free form of the enzyme.



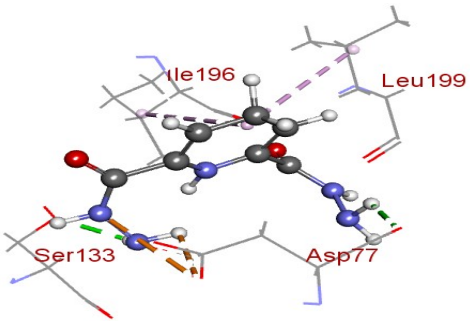
(a) L-Enol (6pnv)



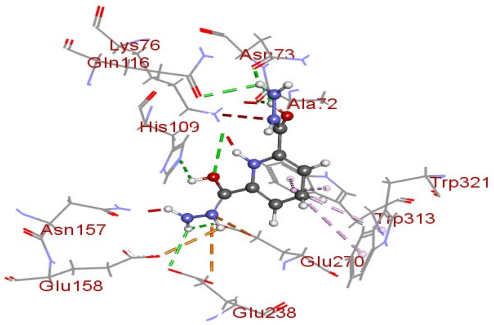
L-Keto (6pnv)



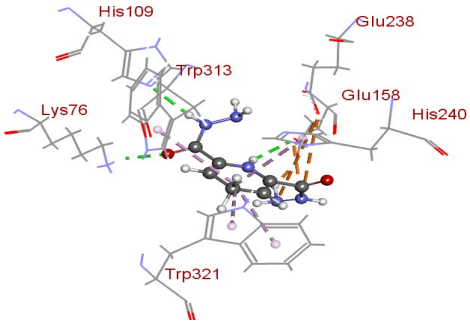
(b) L-Enol (1uwc)



L-Keto (1uwc)



(c) L-Enol (4f8x)



L-Keto (4f8x)

Figure 9. Nonbonding interactions of (A) *Salmonella sp.* (6pnv), (B) *Aspergillus niger* (1uwc), and (C) *Penicillium sp.* (4f8x)

Table 7. *In-silico* antifungal activities against *Aspergillus niger and Penicillium sp.*

Aspergillus niger			
Compounds	**Receptor proteins**	**Binding affinity (Kcal/mol)**	**Residues in Contact, Interaction type (Distance)**
L-Enol	1uwc	-7.1	ASP230, SB(2.75); GLU212, AC(4.97); ASP230, H(2.17); GLY210, H(2.23); CYS227, H(2.19); HIS208, H(2.41).
	3d3z	-6.9	ASP151, SB(2.15); ASP46, H(1.99); GLN34, H(2.83), LEU150, H(2.57); GLN34, H(2.89); SER47, H(3.35).
L-Keto	1uwc	-7.4	ASP77, SB(2.52); ASP77, AC(3.37); ASP77, H(2.07); SER133, H(2.19); ILE196, A(5.21); LEU199, A(5.40).
	3d3z	-6.3	ASP37, AC(2.97); ASP37, H(2.57); TRP36, H(2.64); SER197, H(2.35); PRO40, H(2.30); TYR38, H(2.31); ASP39, H(1.99).
Penicillium sp.			
L-Enol	4f8x	-6.9	GLU158, AC(2.97); GLU238, H(2.49); GLU270, H(2.30); ASN73, H(2.02); GLN116, H(2.59); HIS109, H(2.58).
	1bxo	-6.8	ASP33, AC(2.94); ASP213, AC(4.04); GLU16, AC(4.35); GLY215, H(2.16); ASP77, H(1.99), PHE112, PA(5.06).
	6pvj	-6.5	GLU132, AC(4.52); GLU37, AC(5.31); VAL133, H(2.38); LYS38, H(2.90); VAL133, A(5.33).
	1m7g	-6.3	GLU121, AC(4.87); GLU121, H(1.95); PHE133, H(2.00); PHE7, PA(5.01).
	3a72	-6.4	GLU174, AC(5.33); GLU246, AC(3.14); TYR337, H(2.10); PRO165, A(4.08); TRP173, PA(4.04).
L-Keto	4f8x	-7.7	GLU158, AC(1.97); GLU238, AC(4.66); GLU158, H(2.37); HIS109, H(2.32); LYS76, H(2.13); HIS240, PA(4.26).
	1bxo	-7.0	GLU16, AC(4.33); GLY215, H(2.52); THR217, H(1.96).
	6pvj	-6.9	ASP166, AC(2.27); VAL133, H(1.80); GLU132, H(2.62).
	1m7g	-6.6	GLU121, AC(2.14); PHE133, H(2.38); TYR205, H(2.68); PRO132, A(4.76); PHE7, PA(5.15).
	3a72	-6.4	THR234, H(2.37); LYS235, H(2.17); LEU178, A(4.48); TYR109, PA(5.05); PHE176, PA(5.12).

AC= Attractive charge, H= Conventional H-bond, C= C-H bond, A= Alkyl, SB = Salt bridge, PA= Pi-Alkyl

3.3.8. Antioxidant efficacy

Supplementary Table 2 shows that nearly all of the prepared L and its TM complexes exhibited antioxidant efficacy; i.e., pyridine-2,6-dicarbohydrazide and its transition metal complexes can be exploited as antioxidants. Among them, C5 and C7 complexes have higher phenolic content than others, i.e., indicating more antioxidant activities, showing their reducing ability toward the FCR reagent. The order of antioxidant efficacy is C7>C5>C4>C6>C2>C1>C3>L.

4. Conclusion

This study focuses on the coordination chemistry of the SB-ligand, PDH (L), which was synthesized from PDA and hydrazine hydrate in the presence of concentrated sulfuric acid, and its transition metal complexes. PDH behaves as a tridentate (ONO) dibasic ligand, and its TM complexes were assumed to have tetrahedral geometries in which the fourth coordination number was satisfied by Cl^- in the chromium (Cr^{3+}) complex and H_2O in manganese (Mn^{2+}), iron (Fe^{2+}), cobalt (Co^{2+}), nickel (Ni^{2+}), copper (Cu^{2+}), and zinc (Zn^{2+}) ions which were formed by 1:1 metal-to-ligand ratio. The

prepared ligand and its TM complexes were confirmed by elemental analysis, conductivity, magnetic moment, electronic (UV-Vis), infra-red (IR), proton NMR (for L and C5 complex only) and mass spectrometry. The quantum mechanical studies supported the proposed tetrahedral structures. All of the complexes were screened against bacteria- *Salmonella sp.* fungus- *A. niger,* and *Penicillium sp*. Most of these complexes showed antibacterial and antifungal efficacy. Of them, the C1 complex showed the highest antibacterial efficacy compared with the others, and L, C2, C3, C5, and C6 showed inhibiting activities; C7 showed inducing activity against *A. niger.* Moreover, only inhibiting activities of all the synthesized compounds L and C1-C7 were observed for another fungus, *Penicillium sp.* Antioxidant efficacy was also demonstrated by most of the complexes, and a satisfactory antioxidant activity was observed in all assays.

Acknowledgement

We appreciate the cooperation and insightful suggestions provided by the Laboratory of Advanced Research in Chemical Sciences and Microbiology laboratory of the Department of Chemistry at University of Chittagong in Chattogram, Bangladesh.

Conflict of Interest

The authors state that none of their known competing financial interests or personal connections could have appeared to have an impact on the work that is being published in this paper.

References

[1] Chowdhury, D. A., Uddin, M. N., and Hoque, F. (2010). Dioxouranium (VI) complexes of some bivalent tridentate Schiff-base ligands containing ONS donor set, *Chiang, Mai J. Sci.*, 37, 443-450.

[2] Kaplánek, R., Havlik, M., Dolenský, B., Rak, J., Džubák, P., Konečný, P., Hajdúch, M., Králová, J., Král, V. (2015). Synthesis and biological activity evaluation of hydrazone derivatives based on a Tröger's base skeleton, *Bioorg. Med. Chem,* 23, 1651-1659. https://doi.org/10.1016/j.bmc.2015.01.029.

[3] Al-Ne, M. (2012). Synthesis and characterization of bis-acylhydrazone derivatives as tetradentate ligands and their dinuclear metal (II) complexes, *Period. Pol. Chem. Eng.,* 56, 83-90. https://doi.org/10.3311/pp.ch.2012-2.06.

[4] Nandi, P., Uddin, M. N., Shumi, W., Abida, D., Eshan, T. R., Alam, T., Adan, Z., Nishi, T.A., Alam, S.M.R., Rahman, M.M. (2026). Binuclear metal complexes of a new Schiff base ligand derived from 1,4-diamminobenzene: synthesis, characterization, geometry elucidation, and biological activity, *Results Chem.,* 27, 103391. https://doi.org/10.1016/jrechem.2026.103391.

[5] Zeeshan, M., Kumar, M., Ansari, A., Alarifi, A., Li, X., Ghanem, Y.S.A., Khan, M.Y. (2025). Pyridine-2,4-dicarboxylate as an organic chelating ligand towards cobalt (II) for designing a novel complex: X-ray studies, DFT analysis, and evaluation of catechol oxidase mimic activity and anticancer property towards A549 cell line, *Inorg. Chem. Act.,* 582, 122663. https://doi.org/10.1016/j.ica.2025.122663.

[6] Yenikaya, Cengiz, Poyraz, M., Sari, M., Demirci, F., İlkimen, H. and Büyükgüngör, O. (2009). Synthesis, characterization, and biological evaluation of a novel Cu (II) complex with the mixed ligands 2,6-pyridinedicarboxylic acid and 2-aminopyridine, Polyhedron, 28, 3526-3532. https://doi.org/10.1016/j.poly.2009.05.079.

[7] Uddin, M. N., Begum, S., Akter, J., Ahmed, S. S., Rahman, M. S., Shumi, W. (2022). Ternary complexes of vanadium (IV) and titanium (IV) of Schiff bases as primary ligand: Synthesis, spectral characterization, biomedical applications, and molecular docking with SARS-CoV-2 Mpro, *J. Chinese Chem. Soc.* 69(4), 703-716. https://doi.org/10.1002/jccs.202100319

[8] Jamil, Y.M.S., Al-Azab, F. M., Al-Selwi, N.A., Alorini, T., Al-Hakimi, A.N. (2023). Preparation, physicochemical characterization, molecular docking, and biological activity of a novel Schiff base and

organophosphorus Schiff base with some transition metal (II) ions, *Main Group. Chem.,* 22, 337-362. https://doi.org/10.3233/mgc-220101.

[9] Lee, C., Yang, W., Parr, R. G. (1988). Development of the Colle-Salvetti correlation-energy formula into a functional of the electron density, Phys. Rev., B 37, 785. https://doi.org/10.1103/physrevb.37.785.

[10] Gao, H., Xia, F., Huang, C., Lin, K. (2011). Density functional theory calculations on the molecular structures and vibration spectra of platinum (II) antitumor drugs, *Spectrochim. Acta Part A: Mol. Biomol. Spec.,* 78, 1234-1239. https://doi.org/10.1016/j.saa.2010.12.003.

[11] Sussman, J. L., Dawei, L., Jiansheng, J., Nancy, O. M., Jaime, P., Otto, R., and Enrique, E. A. (1998). Protein Data Bank (PDB): database of three-dimensional structural information of biological macromolecules, *Bio. Crys.,* 54, 1078-1084. https://doi.org/10.1107/s0907444998009378.

[12] Guex, Nicholas, Manual, C. P. (1997). Swiss-model and Swiss-pdb viewer: an environment for comparative protein modeling, *Electrophoresis,* 18, 2714-2723. https://doi.org/10.1002/elps.1150181505.

[13] Uzzaman, M., Junaid, M., Uddin, M. N. (2020). Evaluation of anti-tuberculosis activity of some oxo-titanium (IV) Schiff base complexes: molecular docking, dynamics simulation, ADMET studies, *SN Appl. Sci.,* 2, 880. https://doi.org/10.1007/s424502-020-2644-0.

[14] Dallakyan, Sargis, Arthur, J.O. (2014). Small molecule library screening by docking with PyRx, In Chemical biology: *Methods and Protocols*, (Springer), New York, 243-250.

[15] Uzzaman, M., Shawon, J., Siddique, Z. A. (2019). molecular docking, dynamics simulation, ADMET prediction of acetaminophen and its modified derivatives based on quantum calculations, *SN Appl. Sci.,* 1. https://doi.org/10.1007/s424502-019-1442-z.

[16] Uddin, M. N., Siddique, Z.A., Mase, N., Uzzaman, M., Shumi, W. (2019). Oxotitanium (IV) complexes of some bis-unsymmetric Schiff bases: Synthesis, structural elucidation, and biomedical applications, *Appl. Organomet. Chem.,* 33, e4876. https://doi.org/10.1002/aoc.4876.

[17] Han, Sumin, Liu, Y., and Chang, A., (2007). Cytoplasmic Hsp70 promotes ubiquitination for endoplasmic reticulum-associated degradation of a misfolded mutant of the yeast plasma membrane ATPase, PMA1, *J. Bio. Chem.,* 282, 26140-26149. https://doi.org/10.1074/jbc.m701969200.

[18] Patel, K. S., Kolawole, G. A., (1982). Magnetic and spectral properties of oxovanadium (IV) complexes of quadridentate naphthaldimine ligands, *J. Coord. Chem.,* 11, 231-237. https://doi.org/10.1080/00958978208079742.

[19] Uddin, M. N., Chowdhury, D. A., Hossain, K., (2012). Titanium (IV) complexes of unsymmetrical Schiff bases derived from ethylenediamine and o-hydroxy aldehyde/ketone and their antimicrobial evaluation, *J. Chinese Chem. Soc.,* 59, 1520-1527. https://doi.org/10.1002/jccs.201200169.

[20] Abraham, M. H., Abraham, R. J., Acree, W. E., Aliev, A. E., Leo, A. J., Whaley, W. L. (2014). An NMR method for the quantitative assessment of intramolecular hydrogen bonding: application to physicochemical, environmental and biochemical properties, *J. Org. Chem.,* 79, 11075-11083. https://doi.org/10.1021/jo.502080p.

[21] Uddin, M. N., Amin, M. S., Rahman, M.S., Khandaker, S., Shumi, W., Rahman, M. A., Rahman, S. M. (2021). Titanium (IV) complexes of some tetradentate symmetrical bis-Schiff bases of 1,6-hexanediamine: Synthesis, characterization, in silico prediction of potential inhibitor against coronavirus (SARS-CoV-2), *Appl. Organomet. Chem.,* 35, e6067. https://doi.org/10.1002/aoc.6067.

[22] El-Hamid, S. M. Abd., Sadeek, S. A., Sadek, N. B., Sabry, M. A., El-Gedamy, M. S. (2023). Novel nano-sized metal complexes based on aceclofenac and glycine ligands: Synthesis, characterization, molecular docking studies, and their enhanced efficacy in ameliorating testicular and spermatogical oxidative damages in male rats, *J. Mol. Liq.* 391,123274. https://doi.org/10.1016/j.molliq.2023.123274.

[23] El-Hamid, S. M. Abd., El-Gedamy, M. S., Abdelgawwad, A. M. A., Francés-Monerris, A., Sadeek, S. A. (2026). Synthesis, structural characterization, computational studies, and anticancer evaluation of novel rufloxacin Schiff base metal complexes with involvement of Mcl-1 modulation in breast cancer cells, *J. Trace. Elem. Med. Bio.,* 94, 127851. https://doi.org/10.1016/j.jtemb.2026.127851.

[24] Vinusha, H. M., Kollur, S. P., Rivanasiddappa, H. D., Ramu, R., Shirahatti, P. S., Prasad, M. N. N., Chandreshekar, S., Begum, M. (2019). Preparation, spectral characterization, and biological applications of

Schiff base ligand and its transition metal complexes, *Results Chem.* 1, 100012. https://doi.org/10.1016/j.rechem.2019.100012.

[25] Hasan, M. A., Hossain, M. R., Salam, M. A., Uddin, M. N. (2016). Nickel complexes of Schiff bases derived from mono/diketone with anthranilic acid: synthesis, characterization, and microbial evaluation, *J. Taibah Univ. Sci.,* 10, 766-773. https://doi.org/10.1016/j.jtusci.2015.11.007.

[26] Pardasani, R. T., Pardasani, P., Gupta, A. 2021. *Magnetic properties of paramagnetic compounds: magnetic susceptibility data*, (Vol. 1), (Springer), Berlin, Heidelberg.

[27] Uddin, M. N., Knock, M. N. H., Uzzaman, M., Bhuiyan, M. M. H., Sanaullah, A. F. M., Shumi, W., Amin, H. M. S. (2020). Microwave-assisted synthesis, characterization, molecular docking, and pharmacological activities of some new 2′-hydroxychalcone derivatives, *J. Mol. Struc.* 1206, 127678. https://doi.org/10.1016/j.molstruc.2020.127678.

[28] Saravanan, S., Balachandran, V. (2014). Quantum chemical studies, natural bond orbital analysis, and thermodynamic function of 2,5-dichlorophenylisocyanate, *Spectrochimica Acta Part A: Mol. Biomol. Spec.,* 120, 351-364. https://doi.org/10.1016/j.saa.2013.10.042.

[29] Parr, R. G., and Zhou, Z. (1993). Absolute hardness: unifying concept for identifying shells and subshells in nuclei, atoms, molecules, and metallic clusters, *Acc. Chem. Res.,* 26, 256-258. https://doi.org/10.1021/ar00029a005.

[30] Ayers, P. W., Parr, R. G., Pearson, R. G. (2006). Elucidating the hard/soft acid/base principle: A perspective based on half reactions, *J. Chem. Phys.,* 124. https://doi.org/10.1063/1.2196882.

[31] Azam, F., Abdullah, N. H., Ehmedat, H. M., Abulifa, A. R., Taban, I., Upadhyayula, S. (2018). NSAIDs as a potential treatment option for preventing amyloid β toxicity in Alzheimer's disease: an investigation by docking, molecular dynamics, and DFT studies, *J. Biomol. Struc. Dyn.* 36, 2099-2117. https://doi.org/10.1080/07391102.2017.1338164.

[32] Aihara, J. (1999). Reduced HOMO-LUMO gap as an index of kinetic stability for polycyclic aromatic hydrocarbons, *J. Phys. Chem.* A 103, 7487-7495. https://doi.org/10.1021/jp990092i.

[33] Lipkowitz, K. B., Cundari, T. R. (2007). How computational chemistry became important in the pharmaceutical industry, Rev. Comput. Chem. 23, 401. https://doi.org/10.1002/9780470125847.

[34] Billes, F., Ziegler, I. M. (2007). Vibrational spectroscopy of phenols and phenolic polymers. Theory, experiment, and applications, *Appl. Spec. Rev.* 42, 369-441. https://doi.org/10.1080/00102200701421748.

[35] Uddin, M. N., Ahmed, S. S., Uzzaman, M., Hassan Knock, M. N., Shumi, W., Sanaullah, A. F. M., Bhuyain, M. M. H. (2022). Characterization, molecular modeling and pharmacology of some 2́-hydroxychalcone derivatives as SARS-CoV-2 inhibitor, *Res. Chem.,* 4, 100329 https://doi.org/10.1016/j.rechem.2022.100329.

[36] Uzzaman, M., Chowdhury, M. K., and Hossen, M. B. (2019). Thermochemical, molecular docking, and ADMET studies of aspirin metabolites, Front. Drug. *Chem. Clin. Res.,* 2, 1-5. https://doi.org/10.15761fdccr.1000130.

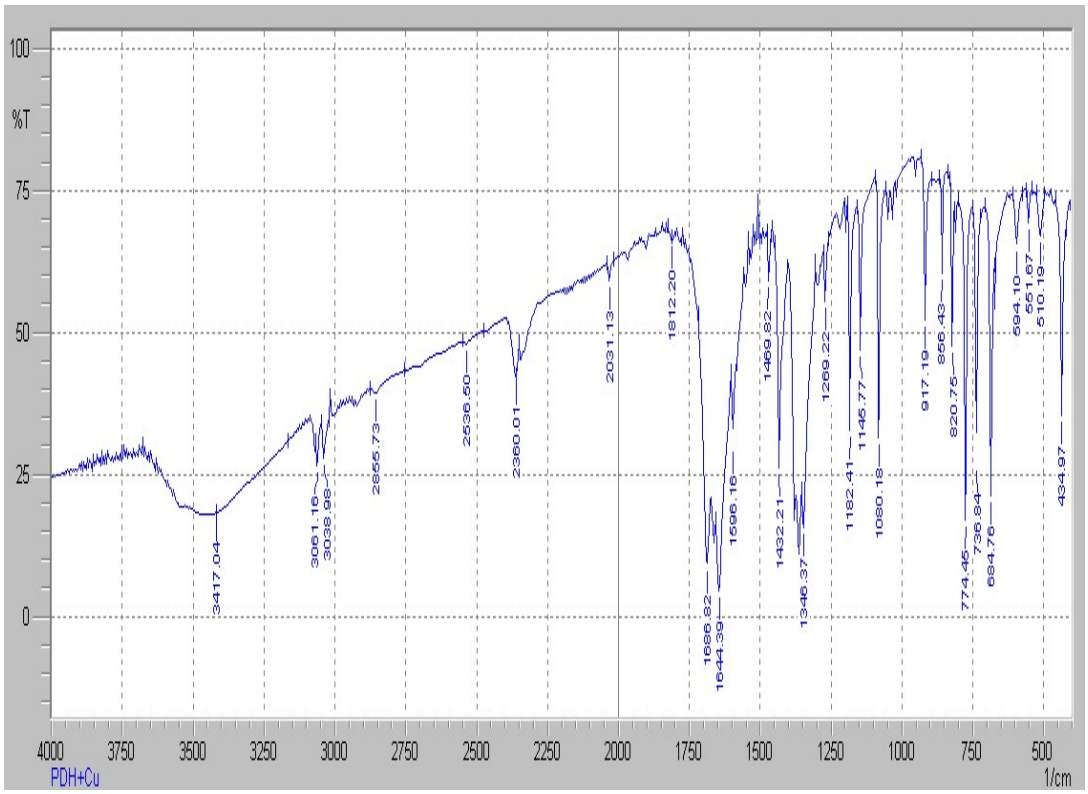
SUPPLEMENTARY INFORMATION

Supplementary Table 1. *In-silico* antibacterial activities against *Salmonella sp.*

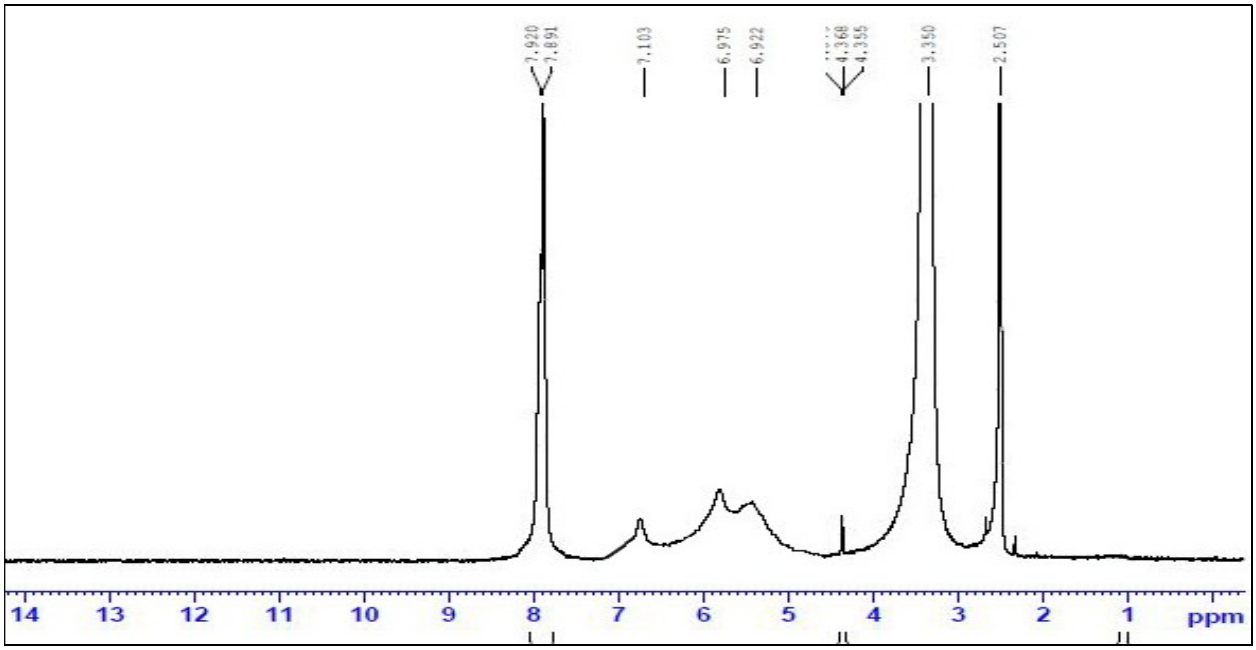
Compounds	Receptor proteins	Binding scores (Kcal/mol)	Residues and interaction type (Distance, Å)
L-Enol	6vnt	-6.9	GLU2, AC(5.08); ASP124, AC(3.31); VAL123, H(2.58); ASN147, H(1.88); ASP124, H(2.01); ALA149, C(2.87).
	6pnv	-7.3	ASP339, SB(2.39); ASP337, AC(4.00); ASP339, AC(4.38); LEU383, H(2.41); TRP427, H(2.91); ASP337, H(2.77).
	1lc5	-6.5	ASP60, AC(2.63); SER247, H(2.70); MET244, H(2.22); ASP60, H(2.23); ALA59, H(2.86); ARG240, A(4.71).
	6h5g	-6.8	ALA222, H(2.14); GLU13, H(2.89); MET15, C(1.97); GLY220, H(2.56); SER221, H(2.48); VAL200, H(2.15).
L-Keto	6vnt	-7.5	GLU2, AC(3.04); GLU5, AC(5.58); ASN147, H(2.35); MET1, H(2.00); ASP124, H(1.99); ARG3, H(2.52); TYR4, H(2.13).
	6pnv	-7.2	VAL340, H(1.95); ASP339, H(2.09); TRP296, H(2.20); LEU383, H(2.22); TRP296, H(2.35); LEU383, H(2.62).
	1lc5	-7.0	ASP190, AC(2.80); ILE189, H(2.39); ILE192, H(2.22); ASP190, H(2.74); GLU195, H(2.44); ARG212, H(2.36).
	6h5g	-6.8	VAL200, H(2.58); GLY220, H(2.33); GLY216, H(2.47); SER221, H(2.53); GLY12, H(2.63).

Supplementary Table 2. Total phenolic contents of tested compounds

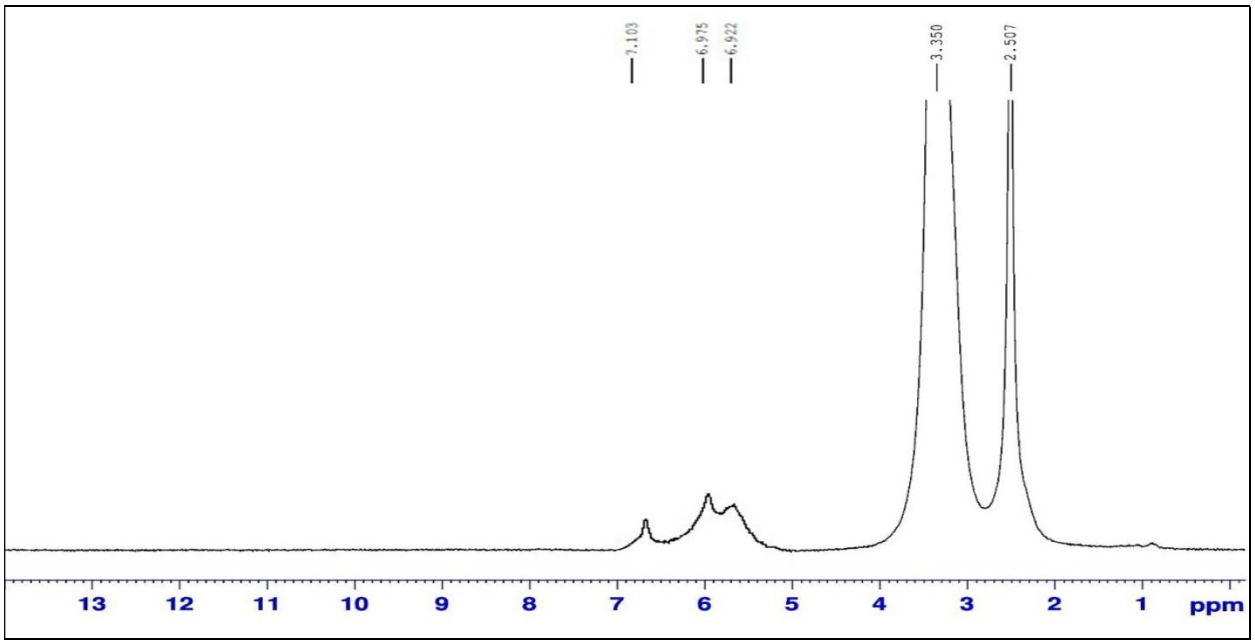
Identification code	Absorbance (nm)	Equivalent Concentration (µg/mL)	Mean	TPC (mg GAE/g dry weight)
L	0.130	127	128.7±1.700	67.74±0.8947
	0.131	128		
	0.134	131		
C1	0.165	162	163.7±1.700	86.16±0.8947
	0.166	163		
	0.169	166		
C2	0.180	177	176.7±0.473	93.00±0.2489
	0.179	176		
	0.180	177		
C3	0.145	142	142.7±2.495	75.11±1.3132
	0.143	140		
	0.149	146		
C4	0.195	192	191.3±1.700	100.68±0.8947
	0.192	189		
	0.196	193		
C5	0.201	198	200±2.828	105.26±1.4884
	0.201	198		
	0.207	204		
C6	0.191	188	186.7±0.943	98.26±0.4963
	0.189	186		
	0.189	186		
C7	0.207	204	202.3±1.557	106.47±0.8194
	0.204	201		
	0.205	202		



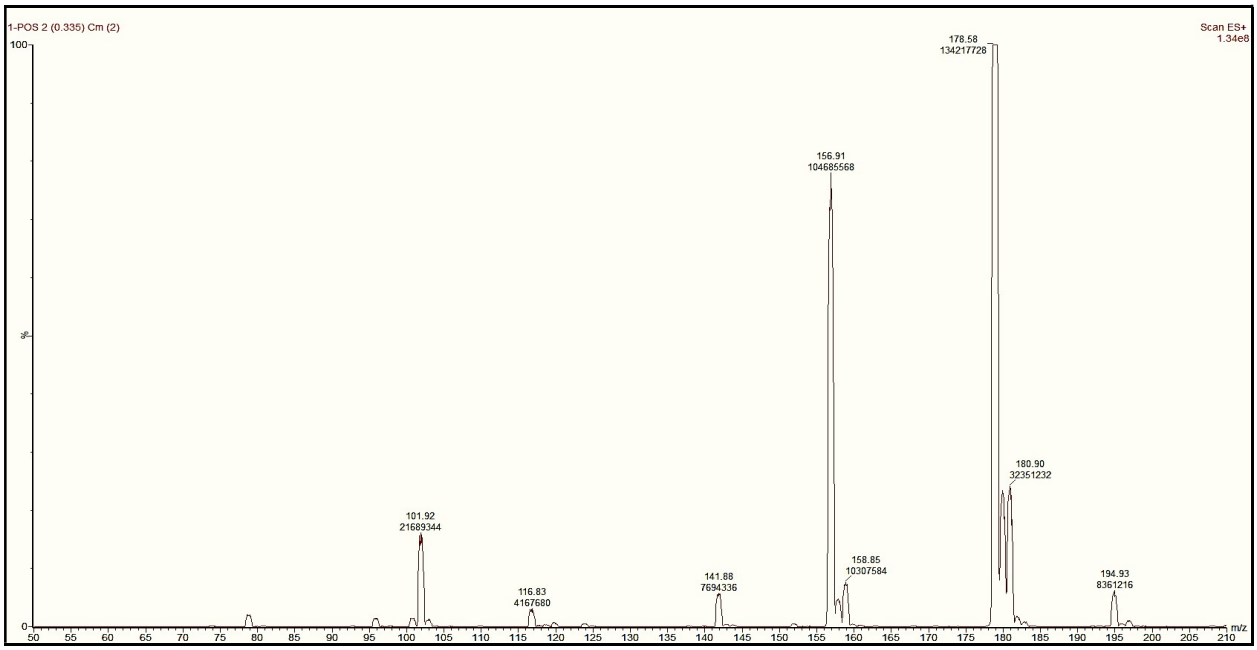
Supplementary Figure 1. IR spectrum of Cu(II) complex, C6.



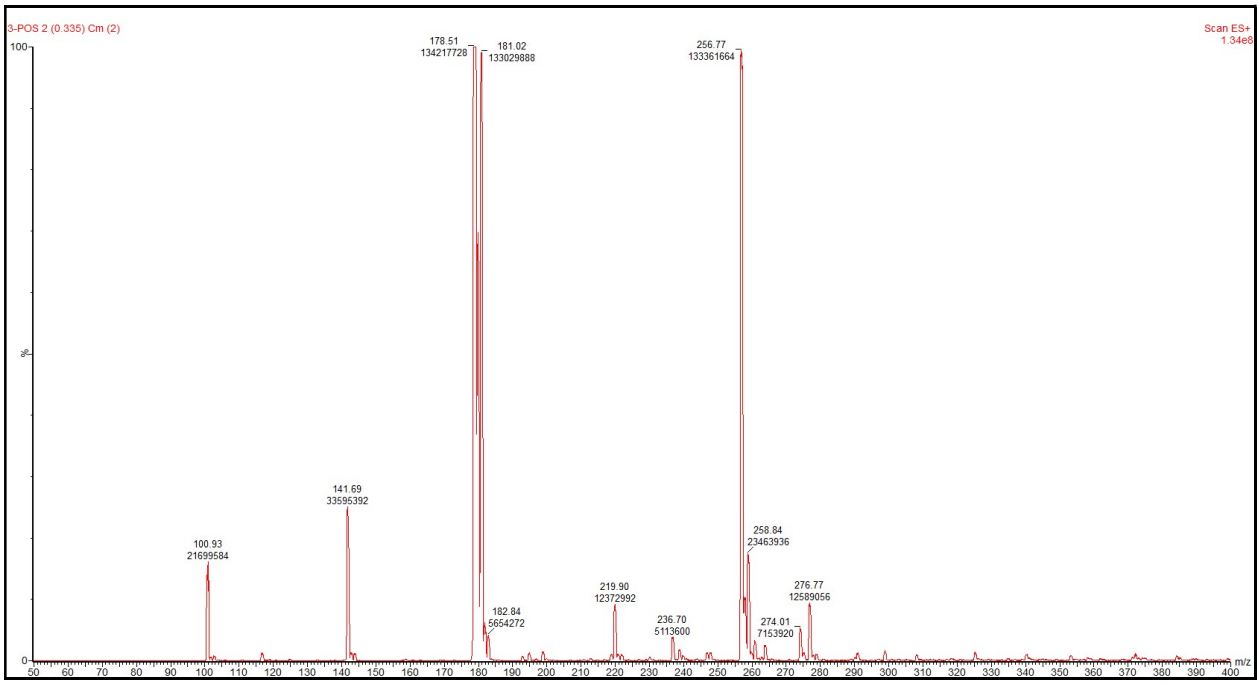
Supplementary.Figure 2. ^{1}H NMR spectrum of Ligand



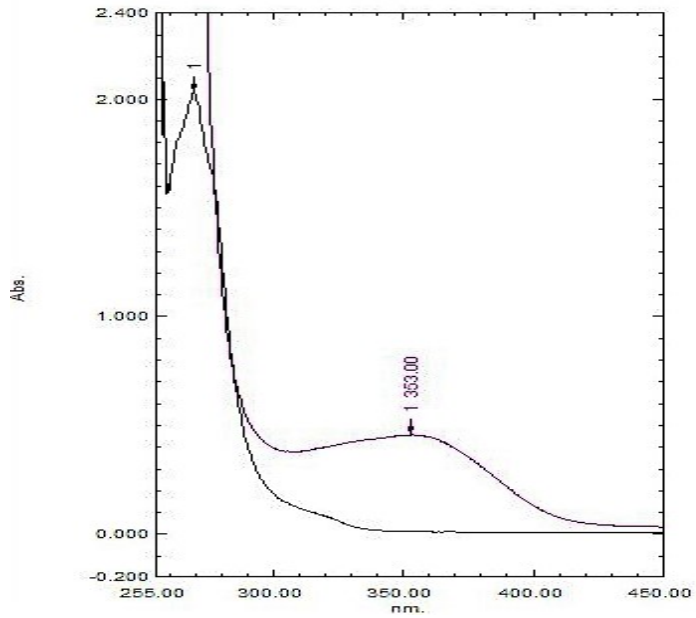
Supplementary Figure 3. ^{1}H NMR spectrum of complex, C5



Supplementary Figure 4. Mass spectrum of Ligand



Supplementary Figure 5. Mass spectrum of complex, C7



Supplementary Figure 6. Electronic spectra of Ligand vs Co(II) complex.